# Water Adsorption on α-Fe₂O₃(0001) at near Ambient Conditions

**Susumu Yamamoto,[†,○] Tom Kendelewicz,[‡] John T. Newberg,[§] Guido Ketteler,[‖,◆] David E. Starr,[§,¶] Erin R. Mysak,[§] Klas J. Andersson,[†,⊥,+] Hirohito Ogasawara,[†] Hendrik Bluhm,[§] Miquel Salmeron,[‖,#] Gordon E. Brown, Jr.,[†,‡] and Anders Nilsson*,[†,⊥,▽]**

*Stanford Synchrotron Radiation Lightsource, 2575 Sand Hill Road, Menlo Park, California 94025, Surface and Aqueous Geochemistry Group, Department of Geological and Environmental Sciences, Stanford University, Stanford, California 94305-2115, Chemical Sciences Division, Lawrence Berkeley National Laboratory, Berkeley, California 94720, Materials Sciences Division, Lawrence Berkeley National Laboratory, Berkeley, California 94720, FYSIKUM, Stockholm University, AlbaNova University Center, SE-10691 Stockholm, Sweden, Department of Materials Science and Engineering, University of California—Berkeley, Berkeley, California 94720, and Stanford Institute for Materials and Energy Sciences, SLAC National Accelerator Laboratory, 2575 Sand Hill Road, Menlo Park, California 94025*

We have investigated hydroxylation and water adsorption on α-Fe₂O₃(0001) at water vapor pressures up to 2 Torr and temperatures ranging from 277 to 647 K (relative humidity (RH) ≤ 34%) using ambient-pressure X-ray photoelectron spectroscopy (XPS). Hydroxylation occurs at the very low RH of $1 \times 10^{-7}$ % and precedes the adsorption of molecular water. With increasing RH, the OH coverage increases up to one monolayer (ML) without any distinct threshold pressure. Depth profiling measurements showed that hydroxylation occurs only at the topmost surface under our experimental conditions. The onset of molecular water adsorption varies from $\sim 2 \times 10^{-5}$ to $\sim 4 \times 10^{-2}$ % RH depending on sample temperature and water vapor pressure. The coverage of water reaches 1 ML at ~15% RH and increases to 1.5 ML at 34% RH.

## 1. Introduction

Iron oxides are central components of many environmental, geological, planetary, and technological processes.[1,2] In natural environments, iron oxides are products of chemical weathering and bacterial processes and are important constituents of rocks and soils. In addition, iron oxides are among the most important environmental sorbents and as such play important roles in determining the composition and quality of natural waters, the mobility of inorganic and organic pollutants, and the availability of plant nutrients in soils.[3] For example, iron oxides play a critical role in the sequestration and release of arsenic in deltaic sediments in Southeast Asia, which is responsible for widespread arsenic pollution of drinking water in this region and impacts the health of 60 million people who live there.[4,5] Iron oxides are also used in a wide range of industrial applications, including heterogeneous catalysis,[6,7] pigments,[8] gas sensors,[9] electrodes for photoelectrochemistry,[10,11] and magnetic materials in data storage devices.[12] A major question concerning the reactivity of iron oxides under humid ambient conditions, where these important environmental processes and technological applications usually occur, is how their interaction with water modifies their surface structure and composition. Most metal oxide surfaces react with water and become partially covered with molecular H₂O and/or its dissociated species OH.[13,14] It is well-known that the presence of water and hydroxyl species on surfaces has a significant influence on the mechanisms and kinetics of surface chemical reactions.[15] Detailed information on in situ surface structure and composition under ambient conditions is therefore essential for a thorough understanding of important chemical reactions on iron oxides in environmental processes and technological applications.

Hematite (α-Fe₂O₃) is the most thermodynamically stable and often the most abundant iron oxide in soils and sediments among a number of other polymorphs of iron oxides and oxyhydroxides.[2,16] Hematite has the corundum crystal structure, with layers of distorted hexagonally close-packed oxygen atoms separated by an iron double layer with Fe³⁺ occupying two-thirds of the octahedral sites in a stacking sequence of −(Fe−O₃−Fe)− along the *c* axis.[17] The (0001) hematite surface is one of the predominant growth faces,[2] and therefore the structure of the α-Fe₂O₃(0001) surface and its interaction with water have been the subject of extensive experimental[18–43] and theoretical[40,44–59] studies [see refs 60 and 61 for reviews on the surface structure of α-Fe₂O₃(0001)].

Three different ideal terminations of the α-Fe₂O₃(0001) surface are known to exist: a single Fe termination (Fe−O₃−Fe−R−), a double Fe termination (Fe−Fe−O₃-R-), and an O termination (O₃−Fe−Fe−R−), where R represents the remaining atomic layers with the bulk stacking sequence (see Figure 1a−c). The most stable surface configuration under ultrahigh vacuum (UHV) conditions has been proposed to be

* Corresponding author. Tel: +1-650-926-2233. Fax: +1-650-926-4100. E-mail: nilsson@slac.stanford.edu.
† Stanford Synchrotron Radiation Lightsource.
‡ Stanford University.
§ Chemical Sciences Division, Lawrence Berkeley National Laboratory.
‖ Materials Sciences Division, Lawrence Berkeley National Laboratory.
⊥ Stockholm University.
# University of California—Berkeley.
▽ SLAC National Accelerator Laboratory.
○ Present address: FOM Institute for Atomic and Molecular Physics (AMOLF), Science Park 113, 1098 XG, Amsterdam, The Netherlands.
◆ Present address: Department of Applied Physics, Chalmers University of Technology, SE-412 96 Göteborg, Sweden.
¶ Present address: Center for Functional Nanomaterials, Brookhaven National Laboratory, Upton, New York 11973.
+ Present address: Center for Individual Nanoparticle Functionality (CINF), Department of Physics, Technical University of Denmark, Fysikvej 312, DK-2800 Kgs. Lyngby, Denmark.
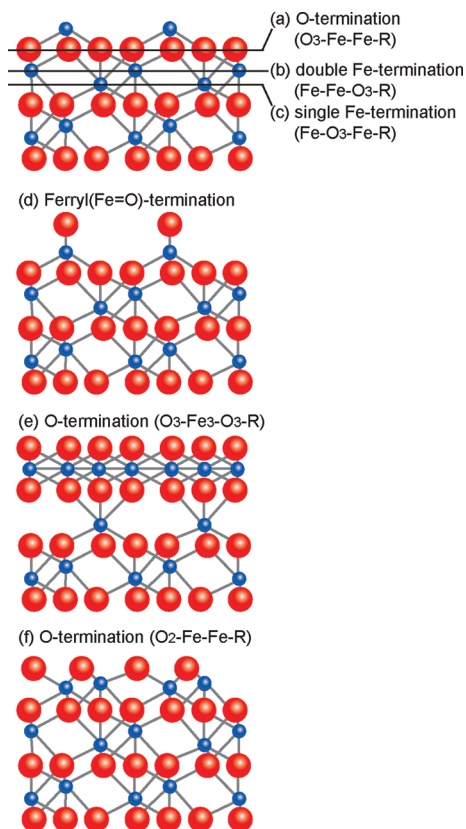
**Figure 1.** Schematic drawing of various surface terminations of the clean α-Fe₂O₃(0001) surface. Large and small spheres represent oxygen and iron atoms, respectively. Note that interlayer spacing and interatomic distance in the figure are for illustration purposes only. The α-Fe₂O₃(0001) surface termination in the present study is tentatively assigned to the single Fe-terminated surface (c); the coexistence of the ferryl-terminated surface (d) is unlikely, but it cannot be fully excluded (see the discussion in the Experimental Section).

the single Fe termination (Fe$-$O₃$-$Fe$-$R$-$) with a highly relaxed structure[31,32,40,43,45,46,51,54] (Figure 1c). Recent experimental studies, however, have shown that the surface termination of α-Fe₂O₃(0001) is sensitive to the sample preparation conditions such as annealing temperatures and oxygen partial pressures. Under oxidizing conditions of high oxygen partial pressures, it has been observed that the single Fe-terminated surface coexists with ferryl termination[41] (O=Fe$-$; Figure 1d), O termination (O₃$-$Fe$-$Fe$-$R$-$),[33,46] or OH termination.[35] Under reducing conditions of low oxygen partial pressures, partial reduction of the surface layer to Fe₃O₄(111),[18,21,23,24,29] Fe$_{1-x}$O(111),[18,21,25,29] or γ-Fe₂O₃(111)[26,27] has been reported. Furthermore, theoretical studies of α-Fe₂O₃(0001) using a combined density functional theory (DFT) and thermodynamics approach predicted different surface terminations as a function of oxygen chemical potential $\mu_o$.[40,41,46,51,54] With a decrease in $\mu_o$ (i.e., lower oxygen partial pressure or higher temperature), various surface terminations were predicted to appear in the following order: O terminations [O₃$-$Fe$-$Fe$-$R$-$[40,46,54] or O₃$-$Fe₃$-$O₃$-$R$-$[51] (see Figure 1e)], ferryl terminations (O=Fe$-$),[41,51,54] and single Fe terminations (Fe$-$O₃$-$Fe$-$R$-$)[40,46,54] or double Fe terminations (Fe$-$Fe$-$O₃$-$R$-$)[51] competing with the reduction to Fe₃O₄. It should be pointed out that there are discrepancies in the relative stabilities of surface terminations depending on the choice of exchange-correlation functionals in DFT. Recently, using in situ surface X-ray scattering technique, Barbier et al.[42] determined the phase stability of different surface terminations on α-Fe₂O₃(0001) as a function of oxygen partial pressure and

temperature. While the O-terminated (O₃$-$Fe$-$Fe$-$R$-$) surface was observed over a wide range of oxygen partial pressures, the ferryl-terminated (O=Fe$-$) surface was found under weaker oxidizing conditions. Reoxidation of the ferryl-terminated surface resulted in the O₂$-$Fe$-$Fe$-$ termination (Figure 1f) accompanied by growth of basal twins. Surprisingly, no evidence was found under the experimental conditions of Barbier et al.[42] ($\mu_o = -1.5$ to $\sim-0.3$ eV) for the formation of the single Fe-terminated surface that has been theoretically predicted as the most stable surface in the corresponding $\mu_o$ regime[46,51,54] and experimentally observed on α-Fe₂O₃(0001) thin films prepared under the stronger oxidizing conditions of oxygen-plasma-assisted molecular beam epitaxy (OPA-MBE).[31,32] Therefore our understanding of the surface phase diagram of α-Fe₂O₃(0001) remains far from complete.

Most of the experimental studies on the α-Fe₂O₃ (0001) surface cited above were carried out in UHV and are therefore ex situ rather than in situ. For example, the ex situ ultraviolet photoemission spectroscopy (UPS) study of water adsorption on α-Fe₂O₃(0001) by Kurtz and Heinrich[20] showed that water molecules adsorbed dissociatively at large water exposures. The ex situ study by Liu et al.[30] investigated the reaction of water with α-Fe₂O₃(0001) in UHV after exposure to different pressures of water vapor using synchrotron-based X-ray photoelectron spectroscopy (XPS). This study found a threshold water pressure of $\sim10^{-4}$ Torr for water dissociation on α-Fe₂O₃(0001). Below the threshold pressure, a small amount of water molecules were dissociated most likely at surface defect sites, whereas above the threshold pressure extensive hydroxylation was observed presumably at surface terrace sites. In that ex situ XPS study, however, the hematite surface was not in equilibrium with water vapor because the XPS measurements were carried out in UHV after exposure of the α-Fe₂O₃(0001) surface to water vapor in a reaction chamber. The surface structure and chemical composition in equilibrium with ambient pressure water vapor can be very different from those in UHV.

The structure of the hydrated α-Fe₂O₃(0001) surface under ambient conditions was studied by Trainor et al. using surface X-ray scattering and ab initio thermodynamic calculations.[40] They showed that the structure and stoichiometry of the α-Fe₂O₃(0001) surface under ambient conditions (relative humidity (RH) > 90% at 298 K) were significantly different from those in UHV. They found that two different hydroxylated domains coexisted on the α-Fe₂O₃(0001) surface under ambient conditions - one corresponding to full hydroxylation of the surface Fe cations ((HO)₃$-$Fe$-$H₃O₃$-$Fe$-$R), and the other to a hydroxylated oxygen layer ((HO)₃$-$Fe$-$Fe$-$R) resulting from the complete removal of the surface Fe cations. However, surface X-ray scattering cannot easily distinguish among different oxygen species such as O, OH, and H₂O in different chemical environments except indirectly through metal$-$oxygen distances. Therefore, until now quantitative information of the in situ chemical composition of α-Fe₂O₃(0001) under ambient conditions has not been available due to the lack of appropriate experimental tools.

In this paper we report an investigation of hydroxylation and water adsorption on α-Fe₂O₃(0001) at near ambient conditions using ambient-pressure X-ray photoelectron spectroscopy (AP-XPS) that provides quantitative information on the in situ chemical composition of surfaces in equilibrium with water vapor in the Torr pressure range. The experiments were performed at pressures ($p(\text{H}_2\text{O}) \leq 2$ Torr) and temperatures ($T = 277-647$ K), covering a relative humidity range of up to 34%.

## 2. Experimental Section

The experiments were performed at the AP-XPS endstation on the undulator beamline 11.0.2 of the Advanced Light Source (ALS) at Lawrence Berkeley National Laboratory, Berkeley, CA. This endstation consists of two interconnected UHV chambers: one for standard surface preparation/characterization and the other for XPS measurements at near ambient pressures. The base pressure in both chambers was about $2 \times 10^{-10}$ Torr.

The single crystal sample of $\alpha$-$Fe_2O_3$ investigated in this study was obtained from a natural mineral crystal (Bahia, Brazil). The sample was cut along a natural (0001) growth face and polished. After polishing, the sample was acid-etched with 0.2 M $HNO_3$ solution and then rinsed with the Milli-Q water. After introduction into the UHV chamber, the sample was cleaned by several cycles of annealing at 723−773 K in $1 \times 10^{-5}$ Torr $O_2$. The sample temperature was monitored by a chromel−alumel (K-type) thermocouple attached to the molybdenum or tantalum plate beneath the sample. The cleaned surface displayed a sharp $(1 \times 1)$ low energy electron diffraction (LEED) pattern, indicative of a high degree of surface order. It should be noted that we chose to avoid ion sputtering, which has often been used for the preparation of iron oxide surfaces.[18,21,23−25,29,39] This was because the LEED pattern substantially deteriorated after sputtering test samples and never recovered by $O_2$ annealing. In addition, ion sputtering of $\alpha$-$Fe_2O_3$(0001) surfaces often leads to partial reduction of the surface layer due to preferential removal of oxygen atoms over iron atoms.[18,21,23−25,29,39]

The $\alpha$-$Fe_2O_3$(0001) surface termination in the present study is tentatively assigned to the single Fe-terminated surface; the coexistence of the ferryl-terminated surface is unlikely, but it cannot be fully excluded. This assignment is based on the following reasoning: (1) The single Fe-terminated surface has been theoretically predicted to be most stable under our sample preparation conditions ($p(O_2) = 1 \times 10^{-5}$ Torr at 723−773 K; $\mu_o = -1.3$ to ∼−1.4 eV).[46,51,54] Furthermore, this termination has been experimentally observed on $\alpha$-$Fe_2O_3$(0001) thin films prepared under more oxidizing conditions.[31,32] (2) The ferryl-terminated surface has been predicted to be most stable in the oxygen chemical potential ranges ($\mu_o = -0.9$ to ∼−0.6 eV,[54] −1.25 to ∼−1.0 eV,[51] and >−1.4 eV[41]), which are rather close to the oxygen chemical potential used in the preparation of our sample ($\mu_o = -1.3$ to ∼−1.4 eV). However, the experimentally observed ferryl-terminated surface was prepared at a much higher oxygen partial pressure and higher annealing temperature ($p(O_2) = 7.5 \times 10^{-3}$∼0.75 Torr at ∼1050 K[41]) than those used in the present study ($p(O_2) = 1 \times 10^{-5}$ Torr at 723−773 K). On balance, we conclude that the coexistence of the ferryl-terminated surface is unlikely, but it cannot be fully excluded. (3) Reduction of $Fe^{3+}$ to $Fe^{2+}$ on the $\alpha$-$Fe_2O_3$(0001) surface can be ruled out because the LEED pattern characteristic of reduced iron oxide surfaces[18,21,23,25−27,29] was not observed. Also no features characteristic of $Fe^{2+}$ species were revealed in Fe 2p XPS and Fe L-edge X-ray absorption spectroscopy (XAS) spectra on our samples.[62−66] (4) The O-terminated ($O_3$−Fe−Fe−R−) surface can be ruled out because our sample preparation conditions are far from the conditions reported for the O-terminated surface ($p(O_2) = 7.5 \times 10^{-1}$∼7.5 $\times 10^{-5}$ Torr at 1100 K[33,46]) and far from the theoretically predicted oxygen chemical potential ranges for the O-terminated surface ($\mu_o > -0.6$ eV[54] and $\mu_o > -1.0$ eV[51]).

XPS measurements at near ambient pressures were carried out using an ambient-pressure XPS setup that combines differential pumping with an electrostatic focusing. The details of the ambient pressure XPS setup have been described in our previous papers.[67−72] Briefly, X-rays were incident on the sample under ambient vapor pressure through a 100 nm thick SiNx window, which separates the ambient pressure chamber from the synchrotron beamline in UHV. The emitted photoelectrons were collected by a small aperture (0.3 mm in diameter) that was the entrance to a differentially pumped electrostatic lens system and were focused on the entrance slit of a hemispherical electron analyzer (Phoibos 150, Specs). The sample was placed close (∼0.5 mm) to the entrance aperture in order to minimize elastic and inelastic scattering of photoelectrons in the gas-phase. This allowed us to carry out in situ XPS measurements at pressures up to a few Torr. The XPS spectra were recorded in an experimental geometry in which the angle between the polarization axis of the incident X-rays and the emitted photoelectrons was set at the magic angle of 54.7°. The incident angle of the X-ray beam and the emission angle of photoelectrons were 20.0° and 42.1°, respectively, with respect to the surface normal. O 1s XPS spectra were measured at a photon energy of 690 eV with a total resolution better than 0.4 eV. There was no need to use a low-energy electron flood gun to neutralize surface charging during the XPS measurements even in UHV because our hematite samples were electrically conductive due to the presence of natural dopants. Water vapor at near ambient pressures was introduced into the chamber through a variable high precision leak valve after being degassed by multiple freeze−pump−thaw cycles of the Milli-Q water.

The surface cleanliness during the experiments was monitored by XPS. After the $O_2$ annealing cycles, carbon contamination was below the detection limit of XPS (<0.01 monolayer (ML)). Under ambient pressure water vapor, however, accumulation of various carbon species such as graphitic carbon and/or hydrocarbon (C−C and/or C−H), methoxy ($CH_3O^-$; C−O), formate ($HCOO^-$; O=C−O) was observed. The total coverage of these various carbon contaminants was estimated to be always below 0.06 (0.04) ML at $p(H_2O) < 0.02$ Torr, 0.13 (0.09) ML at 0.02 Torr, 0.19 (0.10) ML at 0.1 Torr, and 0.36 (0.14) ML at 1 Torr, with the values in parentheses corresponding to the coverage of oxygen-containing carbon species (C−O and O=C−O). In addition, some possibly bulk-derived impurities, such as Si, Mo, and K, were observed on the $\alpha$-$Fe_2O_3$(0001) surface at a level of <0.05 ML after cleaning, while their coverages remained constant during water exposure. The coverage of carbon and other contaminants (i.e., Si, Mo, and K) on $\alpha$-$Fe_2O_3$(0001) is given in units of ML; 1 ML is defined as the surface atomic density of a molecular water layer (i.e., $1.04 \times 10^{15}$ molecules $cm^{-2}$), calculated from the density of bulk liquid water at 298 K ($\rho = 0.997$ g $cm^{-3}$[73]). Further details of coverage calibration for surface contaminants can be found in the Supporting Information.

The O 1s XPS spectra were deconvoluted by mixed Gaussian−Lorentzian functions after a Shirley background subtraction.[74] The O 1s XPS spectra were fit with four peaks corresponding to oxide (Ox), OH, $H_2O$, and oxygen-containing carbon species (C−O and O=C−O). One additional peak was required at water pressures above 0.1 Torr to fit the gas-phase water contribution. In the peak fitting, each peak had four fitting parameters: peak position, full width at half-maximum (fwhm), Lorentzian−Gaussian (L/G) mixing ratio, and intensity. Three parameters (position, fwhm, and L/G ratio) for each component were constrained to be constant unless clear changes were discernible in the raw O 1s XPS spectra. In the present study, as will be shown below, the peak shift of OH and the peak narrowing of Ox were evident in the raw O 1s XPS spectra. The peak position of OH, the fwhm(Ox), and the intensity of

each peak were thus set to be free parameters and optimized in the peak fitting.

To obtain reliable OH and $H_2O$ coverages, it is important to correct the contribution from oxygen-containing carbon species (C—O and O=C—O) in O 1s XPS spectra because O 1s XPS peaks of these carbon species are close to those of OH and $H_2O$.[75] The O 1s XPS intensity of oxygen-containing carbon species was derived from their C 1s XPS intensity using a relative sensitivity factor. The relative sensitivity factor of C 1s to O 1s XPS was experimentally obtained by measuring the O 1s:C 1s XPS intensity ratio of a gas-phase C$x$O$y$ species with a known $x$:$y$ ratio (e.g., $CH_3OH$). Note that O 1s and C 1s XPS spectra were measured with identical kinetic energies to ensure the same lens transmission of the electron spectrometer and the same peak attenuation by the gas-phase. To the best of our knowledge, there are no experimental data on the O 1s XPS peak position of oxygen-containing carbon species on $\alpha$-$Fe_2O_3$ (0001). Therefore, the position and fwhm of the O 1s XPS peak for oxygen-containing carbon species (C—O and O=C—O) on $\alpha$-$Fe_2O_3$(0001) were determined by comparing the O 1s XPS spectrum with a high carbon contamination level ($\theta c$ = 0.64 (0.32) ML) to that with a low carbon contamination level ($\theta c$ = 0.05 (0.03) ML); the values are the total coverage of C contamination (the coverage of oxygen-containing carbon species). [The position and fwhm of the O 1s XPS peak for oxygen-containing carbon species on $\alpha$-$Fe_2O_3$ (0001) were determined to be 531.8 and 1.86 eV, respectively. The changes in these parameters ($\pm$0.2 eV) have a small influence on the coverages of OH and $H_2O$ ($\leq$2%) and the other peak parameters such as fwhm (Ox) and the peak position of OH ($\leq$0.03 eV) at the carbon contamination level ($\theta_c \leq$ 0.36 (0.14) ML) in this study.]

As previously reported,[76,77] water molecules adsorbed on surfaces are susceptible to beam damage (i.e., water dissociation) in X-ray or electron spectroscopies. To minimize the effects of beam damage, great care was taken, including X-ray beam defocusing and changing of sample positions. We did not observe any difference in the coverages of OH and $H_2O$ between spots with extensive X-ray exposure and fresh spots without previous X-ray exposure. Beam-induced damage is thus believed to have been negligible for the results presented here.

## 3. Results and Discussion

Our objective is to understand how hydroxylation and hydration proceed on the $\alpha$-$Fe_2O_3$ (0001) surface as a function of relative humidity (RH) using ambient-pressure XPS. RH was controlled in the following two ways: (1) changing water pressure at constant sample temperature (isotherms) and (2) changing sample temperature at constant water pressure (isobars).

**3.1. Isotherm Results.** First we show O 1s XPS spectra of $\alpha$-$Fe_2O_3$(0001) as a function of water pressure at 295 K (isotherm). In Figure 2, the O 1s XPS spectra at selected water pressures and the results of peak fitting are presented. The binding energy (BE) of O 1s XPS spectra was calibrated by fixing the oxide peak at 530.0 eV.[63,64,78−81] At the lowest pressure of 2 × 10$^{-9}$ Torr before introducing water vapor, a broad oxide (Ox) peak[63,64,78−81] is observed with a small shoulder centered at 531.2 eV. A similar shoulder feature with a chemical shift of 1.0−1.3 eV from the Ox peak was often observed on clean iron oxide surfaces in UHV.[82−84] This feature has been suggested to be due to nonstoichiometric oxygens or hydroxyl species formed by residual water in the vacuum chamber or to final-state effects such as shake-up, but it is still under debate.[82−84]
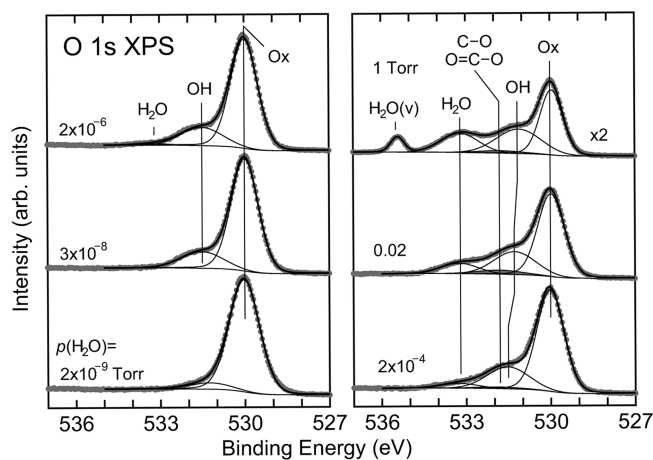


**Figure 2.** O 1s XPS spectra of $\alpha$-$Fe_2O_3$(0001) as a function of water pressure at 295 K. The incident photon energy was 690 eV. The binding energy of the oxide (Ox) peak is fixed at 530.0 eV. The experimental data are shown as gray dots and the results of the peak fitting are shown as solid black lines. Note that the O 1s XPS spectrum at 1 Torr is enlarged by a factor of 2 for clarity. As water pressure increases, hydroxyl (OH) and molecular water ($H_2O$) are observed on the $\alpha$-$Fe_2O_3$(0001) surface. At 1 Torr, a gas-phase water ($H_2O$(v)) is observed. The contribution from oxygen-containing carbon species (C—O and O=C—O) to the O 1s XPS spectra is shown as a shaded peak.

When the surface is exposed to 3 × 10$^{-8}$ Torr of water vapor, a significant shoulder is observed at ~531.5 eV. This peak is assigned to surface hydroxyl (OH) species on $\alpha$-$Fe_2O_3$, in good agreement with the reported BE values of OH.[28,32,63] At a water pressure of 2 × 10$^{-6}$ Torr, an additional broad peak appears at ~533.2 eV, which is assigned to adsorbed molecular water.[28,83,85] With further increase in water pressure, the intensities of both the OH and $H_2O$ peaks increase. At 0.1 (not shown) and 1 Torr, a peak due to gas phase water is observed at ~535.5 eV. At these high vapor pressures, the XPS peaks of surface species are attenuated in intensity due to the scattering of photoelectrons by gas phase molecules. The peak position of the OH feature shifts to lower BE's at $p(H_2O) \geq$ 0.02 Torr (see Figure 2); the chemical shift of OH with respect to the Ox peak (i.e., $\Delta E$(OH-Ox)) decreases from 1.51 eV (at $p(H_2O)$ = 3 × 10$^{-8}$~5 × 10$^{-4}$ Torr) to 1.29 eV (0.02 Torr), 1.26 (0.1 Torr), 1.17 eV (1 Torr). In addition, the width of the Ox peak decreases with increasing water pressure from 1.13 eV (at $p(H_2O)$ = 3 × 10$^{-8}$~5 × 10$^{-4}$ Torr) to 1.11 (0.02 Torr), 1.10 (0.1 Torr), 0.95 eV (1 Torr). Note that the chemical shift and fwhm of the $H_2O$ peak remain constant as water pressure increases.

**3.2. Isobar Results.** Figure 3a shows O 1s XPS spectra of $\alpha$-$Fe_2O_3$(0001) as a function of sample temperature at 1 Torr water vapor pressure (isobar). The OH and $H_2O$ features in the isobar exhibit spectral changes similar to those in the isotherm shown in Figure 2. At the highest temperature (553 K, the rear spectrum), the broad Ox peak is observed with the OH shoulder at ~531.5 eV. As temperature decreases to 283 K (moving from the rear to the front spectra), the $H_2O$ peak appears at ~533.2 eV and increases in intensity. The changes in O 1s XPS spectral features are highlighted in Figure 3b, which compares the O 1s XPS spectra at the highest and lowest temperatures; the OH peak shifts to lower BE's with decrease in temperature ($\Delta E$(OH-Ox) = 1.58 eV at 553 K and 1.03 eV at 283 K). In addition, the width of the Ox peak is decreased from 1.15 eV at 553 K to 0.92 eV at 283 K. The chemical shift and fwhm of the $H_2O$
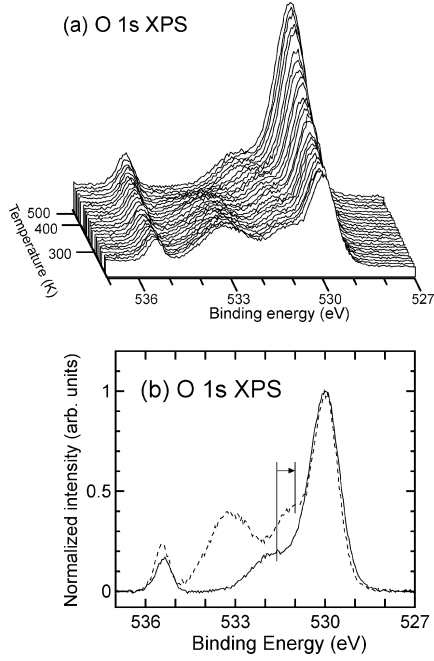
**Figure 3.** (a) O 1s XPS spectra of α-Fe$_2$O$_3$(0001) recorded in the presence of 1 Torr water vapor as a function of sample temperature. From the rear to the front, the sample temperature decreases from 553 to 283 K. The incident photon energy was 690 eV. The binding energy of the Ox peak is fixed at 530.0 eV. (b) Comparison of the O 1s XPS spectra in (a) measured at the highest temperature of 553 K (solid line) and at the lowest temperature of 283 K (dashed line). Note that the spectra in (b) are normalized with the intensity of the Ox peak after a Shirley background subtraction. In addition to the appearance of water peak at ∼533.2 eV, the OH peak shifts to lower binding energies and the width of the Ox peak decreases.

peak remain constant as the temperature decreases. These changes in O 1s XPS spectral features will be discussed in detail below.

**3.3. Coverage Calibration.** In order to obtain quantitative insight into hydroxylation and hydration of α-Fe$_2$O$_3$ (0001), the coverages of OH and H$_2$O were estimated from the O 1s XPS spectra using a multilayer electron attenuation model.[75,86,87] In this model, the water-dosed α-Fe$_2$O$_3$ (0001) surface is represented by a multilayer interface, from top to bottom, as H$_2$O/OH/Fe$_2$O$_3$(Ox); the bulk oxide (Ox) substrate is covered by a hydroxylated (OH) layer of thickness $t_{OH}$, and an adsorbed water (H$_2$O) layer of thickness $t_{H_2O}$. The OH and H$_2$O overlayers are assumed to be distributed uniformly across the XPS analysis area with constant density and thickness. The contribution from oxygen-containing carbon species (C−O and O=C−O) in O 1s XPS spectra was corrected as described in the Experimental Section.

In general, the intensity of the XPS peak from a specific component $i$ of thickness $t_i$ is given by:

$$I_i \sim D_i\beta_i\Phi_iN_i\sigma_i \int_0^{t_i} \exp\left(-\frac{z}{\lambda'_i}\right) dz$$

$$= D_i\beta_i\Phi_iN_i\sigma_i\lambda'_i\left(1 - \exp\left(-\frac{t_i}{\lambda'_i}\right)\right) \quad (1)$$

where $D$ is the spectrometer efficiency for a given kinetic energy (KE), $\beta$ is the asymmetry parameter, $\Phi$ is the X-ray photon flux, $N$ is the atomic density, $\sigma$ is the atomic photoionization cross section, $\lambda' = \lambda \cos\theta$ ($\lambda$ is the inelastic mean free path

(IMFP) of photoelectrons, and $\theta$ is the emission angle of photoelectrons from the surface normal).

In O 1s XPS spectra, the parameters such as $D$, $\beta$, and $\Phi$ are constant and cancel out when taking the ratio of different components. Thus the XPS intensity $I_{H_2O}$ from adsorbed water is given by

$$I_{H_2O} \sim N_{H_2O}\sigma_{H_2O}\lambda'_{H_2O}\left(1 - \exp\left(-\frac{t_{H_2O}}{\lambda'_{H_2O}}\right)\right) \quad (2)$$

The XPS intensity $I_{OH}$ from hydroxyl species is given by a similar expression except that the escape probability is multiplied by the attenuation factor $\exp(-t_{H_2O}/\lambda'_{H_2O})$ of the water overlayer

$$I_{OH} \sim N_{OH}\sigma_{OH}\lambda'_{OH}\left(1 - \exp\left(-\frac{t_{OH}}{\lambda'_{OH}}\right)\right)\exp\left(-\frac{t_{H_2O}}{\lambda'_{H_2O}}\right) \quad (3)$$

The XPS intensity $I_{Ox}$ from an oxide substrate (Ox) is attenuated by both the OH and H$_2$O layers

$$I_{Ox} \sim N_{Ox}\sigma_{Ox}\lambda'_{Ox}\exp\left(-\frac{t_{OH}}{\lambda'_{OH}}\right)\exp\left(-\frac{t_{H_2O}}{\lambda'_{H_2O}}\right) \quad (4)$$

By taking the intensity ratio of OH to Ox, the thickness of the OH layer is calculated from

$$t_{OH} = \lambda'_{OH}\ln(1 + R_{Ox}^{OH}) \quad (5)$$

where

$$R_a^b = \frac{I_b}{I_a}\left(\frac{N_a\sigma_a\lambda'_a}{N_b\sigma_b\lambda'_b}\right)$$

Similarly, the thickness of the H$_2$O layer is obtained by taking the intensity ratio of H$_2$O to Ox

$$t_{H_2O} = \lambda'_{H_2O}\ln\left(1 + R_{Ox}^{H_2O}\exp\left(-\frac{t_{OH}}{\lambda'_{OH}}\right)\right) \quad (6)$$

The thicknesses of the OH and H$_2$O layers ($t_{OH}$ and $t_{H_2O}$) are thus calculated from the intensity ratio of OH or H$_2$O to the Ox peak determined by fitting the experimental O 1s XPS spectra as well as the values of the parameters $N_i$, $\sigma_i$, $\lambda_i$, and $\theta$. The details of peak fitting procedures for O 1s XPS spectra are described in the Experimental Section. The fitting parameters of O 1s XPS spectra are summarized in Table 1. It should be noted that eqs 5 and 6 are also valid at ambient conditions where the XPS intensities from surface species are equally attenuated by gas-phase molecules, because the gas-phase attenuation is canceled out when taking the ratio of OH or H$_2$O to Ox.

In the present multilayer model, the hydroxylated and adsorbed water layers on the α-Fe$_2$O$_3$(0001) surface are modeled by bulk α-FeOOH (goethite) and bulk liquid water, respectively. The atomic densities of the hydroxylated layer, $N_{OH}$, and the oxide layer, $N_{Ox}$, are obtained from the density of bulk α-FeOOH ($\rho = 4.26$ g cm$^{-3}$ [73]) and bulk α-Fe$_2$O$_3$ ($\rho = 5.25$ g cm$^{-3}$ [73]),

**TABLE 1: Summary of O 1s XPS Spectral Features for Surface Species on α-Fe₂O₃(0001)[a]**

| species | BE (eV) | fwhm (eV) | L/G (%)[b] |
|---|---|---|---|
| Ox | 530.00[c] (0) | 1.15−0.92[d,e] | 10 |
| OH | 531.58−530.97[d,e] (1.58−0.97) | 1.82[e] | 0 |
| H₂O | 533.25[e] (3.25) | 1.52[e] | 0 |
| C−O, O=C−O | 531.82[f] (1.82) | 1.86[f] | 0 |

[a] The fitting parameters are reported for the surface species on α-Fe₂O₃(0001) including oxide (Ox), OH, H₂O, and oxygen-containing carbon species (C−O and O=C−O): Binding energy (BE) (the values in the parentheses are chemical shift from Ox peak), full width at half-maximum (fwhm), Lorentzian- Gaussian (L/G) mixing ratio. [b] L/G is a parameter of linear combination of Lorentzian and Gaussian; L/G = 0 for 100% Gaussian and L/G = 1 for 100% Lorentzian. [c] The binding energy of oxide (Ox) peak was fixed at 530.00 eV. [d] The peak shift of OH to lower BE and the peak narrowing of Ox were observed as RH increases (see the main text for details). [e] Typical variations between different data sets were less than ±0.05 eV for BE's of OH and H₂O and less than ±0.07 eV for fwhm's of OH and H₂O. [f] The peak position and fwhm of oxygen-containing carbon species (C−O and O=C−O) were experimentally determined (see the experimental section for details).

respectively; $N_{OH} = 5.77 \times 10^{22}$ cm$^{-3}$, $N_{Ox} = 5.94 \times 10^{22}$ cm$^{-3}$. The atomic density of adsorbed water, $N_{H_2O}$, is assumed to be that of bulk liquid water at 298 K ($\rho = 0.997$ g cm$^{-3}$ [73]); $N_{H_2O} = 3.33 \times 10^{22}$ cm$^{-3}$. The photoionization cross sections, $\sigma$, for oxide, OH, and H₂O are constant. The IMFP for each layer is calculated using the NIST IMFP database (#71)[88] with the Tanuma−Penn−Powell method (TPP-2M) equation.[89] The IMFP of an electron in a solid depends on its kinetic energy. In the O 1s XPS spectra measured with an incident photon energy of 690 eV, for example, the kinetic energy of O 1s XPS photoelectrons is about 155 eV. At 155 eV, the IMFP for each layer in the H₂O/OH/Fe₂O₃(Ox) system is as follows: $\lambda_{H_2O} = 0.967$ nm, $\lambda_{OH} = 0.677$ nm, and $\lambda_{Ox} = 0.625$ nm. [In the TPP-2 M equation to calculate IMFP for each layer, the following parameter values were used; band gap ($E_g$), density ($\rho$), and the number of valence electrons ($N_v$). H₂O: $E_g = 6.9$ eV,[90] $\rho = 0.997$ g cm$^{-3}$,[73] $N_v = 8$. α-FeOOH (OH): $E_g = 2.1$ eV,[91] $\rho = 4.26$ g cm$^{-3}$,[73] $N_v = 21$. α-Fe₂O₃ (Ox): $E_g = 2.2$ eV,[2] $\rho = 5.25$ g cm$^{-3}$,[73] $N_v = 34$.] The emission angle of photoelectrons from the surface normal, $\theta$, was fixed at 42.1° in this study. The calculated thicknesses of the OH and H₂O layers are converted into coverage in monolayer (ML) units by dividing by the following definitions of 1 ML thickness for each component. One ML of adsorbed water is defined as an average thickness of a molecular layer in bulk liquid water (0.31 nm), which is the cubed-root of bulk liquid water density at 298 K ($\rho = 0.997$ g cm$^{-3}$ [73]). One ML of hydroxyls is defined using the lattice constant of bulk α-FeOOH ($b = 0.3021$ nm).[2]

It is appropriate to discuss possible limitations in the multilayer model used in this study for the coverage calibration of OH and H₂O. As mentioned earlier, uniform layers of OH and H₂O are assumed in the present multilayer model. The adsorbed water layer, however, may grow as three-dimensional islands. Recent experimental and theoretical studies showed that the adsorbed water layers on oxides and carbonates can be quite nonuniform.[92−94] A detailed discussion on the morphology of the adsorbed water layer would require additional measurements by microscopic methods with a spatial resolution such as
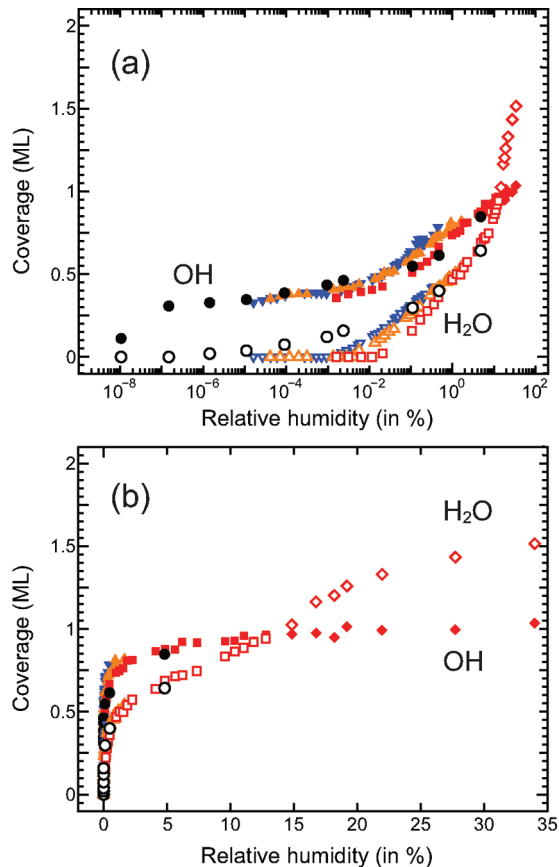


**Figure 4.** Coverages of OH and H₂O on α-Fe₂O₃(0001) as a function of relative humidity (RH). To enlarge the low and high RH regions, the RH on the *x*-axis is plotted on a logarithmic scale in (a), and on a linear scale in (b). RH is defined as $p'/p_v(T) \times 100$, where $p_v$ is the equilibrium vapor pressure of bulk water at the sample surface temperature. The influence of the temperature difference between gas and surface on RH in isobar experiments is corrected in $p'$ (see the text for details). The coverages of OH (filled symbols) and H₂O (open symbols) are obtained from an isotherm ($T = 295$ K) (circles in black) and three different isobars; $p(H_2O) = 0.02$ Torr (down-pointing triangles in blue), 0.1 Torr (up-pointing triangles in orange), 1 Torr (squares in red). In addition, the high RH data measured at $p(H_2O) = 1.0−2.0$ Torr and $T = 280−277$ K (diamonds in red) are included in the figure.

scanning tunneling microscopy. In addition, one may question if the surface hydroxyl layer on α-Fe₂O₃(0001) can be represented by bulk α-FeOOH. Although goethite (α-FeOOH) is the most stable iron oxyhydroxide and the transformation of hematite (α-Fe₂O₃) to goethite (α-FeOOH) is thermodynamically favorable in bulk,[2,16] the formation of α-FeOOH has not been experimentally observed on the α-Fe₂O₃ surface under ambient conditions and in contact with liquid water.[22,28] However, the OH chemical shift of α-Fe₂O₃(0001) at high RHs in the present study agrees well with previously reported OH chemical shifts of α-FeOOH (1.1−1.3 eV)[78−81,95] Furthermore, as the thickness of one hydroxylated layer (0.3021 nm) in the present model is close to the diameter of an OH group (0.27 nm),[96] using α-FeOOH as a model for the hydroxylated α-Fe₂O₃(0001) surface is a reasonable approximation.

**3.4. Uptake of OH and H₂O: Comparison of Isotherm and Isobar Data.** Figure 4 compares the uptake curves of OH and H₂O on α-Fe₂O₃(0001) obtained from one isotherm at 295 K and three isobars at different water pressures (0.02, 0.1, and 1 Torr). Also included in Figure 4 are the high RH data measured at $p(H_2O) = 1.0−2.0$ Torr and $T = 280−277$ K. The coverages of OH and H₂O are plotted as a function of RH. RH is plotted

on a logarithmic scale in Figure 4a and on a linear scale in Figure 4b to enlarge the low and high RH regions, respectively. RH is defined as $p'/p_v(T) \times 100$, where $p_v$ is the equilibrium vapor pressure of bulk water[73] at the sample surface temperature. In isobar experiments, the temperature of the gas ($T_{gas}$) was room temperature and was different from the surface temperature ($T_{surf}$). Using $T_{surf}$ to calculate RH is thus not strictly correct. In this study the error in RH induced by using $T_{surf}$ is corrected in the following way. In adsorption−desorption equilibrium, the rates of adsorption and desorption are equal. The rate of adsorption is proportional to the incident flux, which depends on the gas pressure, $p$, and $T_{gas}$ as $p/\sqrt{T_{gas}}$; the rate of desorption depends on $T_{surf}$ as $\exp(-E/kT_{surf})$. One can see that $T_{surf}$ is a dominant factor that determines adsorption−desorption equilibrium. In addition, if $T_{gas}$ is not equal to $T_{surf}$ (i.e., in isobars), only the rate of adsorption is affected, which leads to the change in the gas pressure in adsorption−desorption equilibrium as $p' = p(T_{gas}/T_{surf})^{1/2}$. This corrected gas pressure, $p'$, was used to calculate RH in this study.

The uptake curve of OH shows that hydroxylation of $\alpha$-Fe$_2$O$_3$(0001) occurs at the very low RH of $\sim 1 \times 10^{-7}$ % (see Figure 4a). The OH coverage then increases slowly between $1 \times 10^{-7}$ and $\sim 10^{-3}$ % RH. Above $\sim 10^{-3}$ % RH, which coincides with the onsets of water adsorption, the OH coverage increases more rapidly and approaches 1 ML at the maximum RH of 34% (see Figure 4b).

In the uptake curve of H$_2$O, the onsets of water adsorption are different for the isobars and the isotherm. Here the onset of water adsorption is defined as the point at which the coverage of adsorbed H$_2$O is 0.05 ML. The onset of water adsorption in the isotherm at 295 K is at $\sim 2 \times 10^{-5}$ % RH ($p$(H$_2$O) $\approx 5 \times 10^{-6}$ Torr), while the onsets in the isobars are observed at higher RH's. In addition, the onset of water adsorption is observed at higher RH's as water pressure in the isobar increases as follows: $\sim 4 \times 10^{-3}$ % RH ($p$(H$_2$O) = 0.02 Torr at $\sim 369$ K), $\sim 7 \times 10^{-3}$ % RH ($p$(H$_2$O) = 0.1 Torr at $\sim 388$ K), and $\sim 3 \times 10^{-2}$ % RH ($p$(H$_2$O) = 1 Torr at $\sim 416$ K). The coverage of water increases rapidly with an inflection point at $\sim 0.75$ ML at $\sim 8\%$ RH, and reaches 1 ML at $\sim 15\%$ RH and 1.5 ML at the maximum RH of 34% in this study.

**3.5. Depth Profiling.** The depth distribution of the various chemical species on $\alpha$-Fe$_2$O$_3$(0001) was investigated using depth profiling by variation of incident photon energy. Because the IMFP of an electron in a solid depends on its kinetic energy (KE), the probing depth in XPS can be varied with the incident photon energy (h$\nu$); KE = h$\nu$ − BE − $\Phi$ (where $\Phi$ is work function). Figure 5a shows O 1s XPS spectra of $\alpha$-Fe$_2$O$_3$(0001) recorded in the presence of 1 Torr water vapor at 295 K ($\sim 5\%$ RH) as a function of incident photon energy. All the spectra are normalized to the intensity of the Ox peak at 530.0 eV after a Shirley background subtraction to clearly show spectral changes with depth profiling. The incident photon energy was varied from 660 to 900 eV (from $\sim 125$ to $\sim 365$ eV in KE), which leads to an IMFP range from 0.579 to 0.988 nm in the case of Fe$_2$O$_3$.[88] As seen in Figure 5a, the intensities of the OH and H$_2$O peaks relative to the Ox peak decreases as the incident photon energy (i.e., the probing depth) increases. These changes indicate that OH and H$_2$O are located at the $\alpha$-Fe$_2$O$_3$(0001) surface. Figure 5b presents the coverages of OH and H$_2$O on $\alpha$-Fe$_2$O$_3$(0001) calculated from the O 1s XPS spectra in Figure 5a using the multilayer model. The coverages of OH and H$_2$O appear to be constant at 0.90 ± 0.05 and 0.72 ± 0.01 ML, respectively, regardless of probing depth. The depth-profiling experiment thus shows that hydroxylation on $\alpha$-Fe$_2$O$_3$(0001)
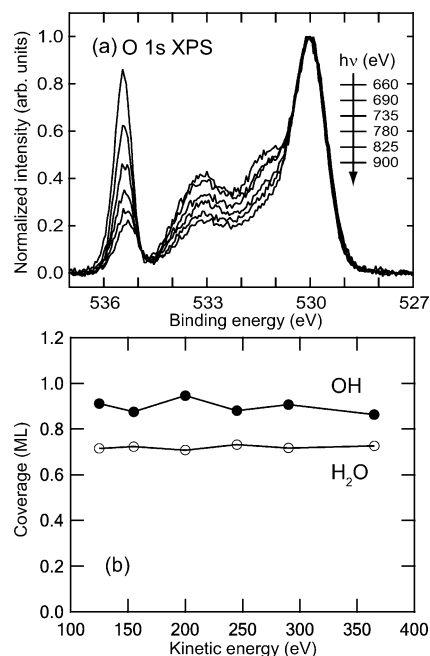


**Figure 5.** (a) O 1s XPS spectra of $\alpha$-Fe$_2$O$_3$(0001) recorded in the presence of 1 Torr water vapor at 295 K as a function of incident photon energy. With an increase in the incident photon energy, the probing depth is increased because the inelastic mean free path (IMFP) of the emitted photoelectron is increased. All the spectra are normalized with the intensity of the Ox peak at 530.0 eV after a Shirley background subtraction. (b) Coverages of OH and H$_2$O on $\alpha$-Fe$_2$O$_3$(0001) under 1 Torr water vapor at 295 K obtained from O 1s XPS spectra in (a) with different probing depths using a multilayer model. In the peak fitting of O 1s XPS spectra in (a), the chemical shifts for OH and H$_2$O from the Ox peak were kept constant; the fwhm ratio of OH and H$_2$O to Ox was kept constant to take into consideration the fact that spectral resolution decreases with increasing the incident photon energy.

under the present experimental conditions is limited to the topmost surface.

**3.6. Discussion. 3.6.1. Uptake Curves of OH and H$_2$O on $\alpha$-Fe$_2$O$_3$(0001).** First we discuss the uptake curves of OH and H$_2$O on $\alpha$-Fe$_2$O$_3$(0001). The hydroxylation on $\alpha$-Fe$_2$O$_3$(0001) occurs at the very low RH of $1 \times 10^{-7}$ % ($3 \times 10^{-8}$ Torr at 295 K). The coverage of OH increases with an increase in RH, and increases more rapidly after the onset of water adsorption. This may be attributed to a cooperative effect among adsorbed water molecules, resulting in water dissociation as reported for metals[97] and oxides.[98−100] The water-catalyzed dissociation is explained by the stabilization of the dissociated final state due to the strong hydrogen bond between H$_2$O and OH, which lowers the kinetic barrier for water dissociation.[97] At high RH's the $\alpha$-Fe$_2$O$_3$(0001) surface is covered with 1 ML of OH species. This maximum coverage of OH is consistent with previous studies where 1 ML of hydroxyl species was observed on hematite powders exposed to ambient pressure water vapor[101,102] and on the $\alpha$-Fe$_2$O$_3$(0001) single crystal exposed to air or immersed in bulk water.[28]

The onset of water adsorption varies from $\sim 2 \times 10^{-5}$ to $\sim 4 \times 10^{-2}$ % RH depending on sample temperature and water pressure. In Figure 4, it should be noted that at the same RH the data points from the isobars are measured at much higher temperatures than the isotherm at 295 K. For example, at $\sim 2 \times 10^{-3}$ % RH the data point from the isotherm at 295 K was measured in $\sim 4 \times 10^{-4}$ Torr water vapor, whereas the data point from the 1 Torr isobar was measured at $\sim 535$ K. The different onsets of water adsorption between the isobars and
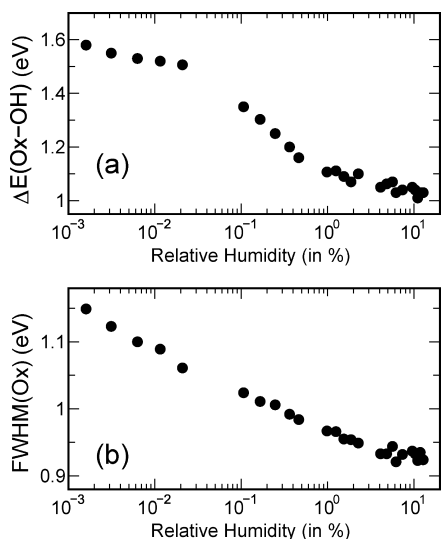
**Figure 6.** (a) Chemical shift of OH species relative to oxide (Ox) as a function of RH. (b) Full width half-maximum (fwhm) of the Ox peak as a function of RH. The data are derived from the O 1s XPS spectra on $\alpha$-Fe$_2$O$_3$(0001) recorded in the presence of 1 Torr water vapor as a function of sample temperature as shown in Figure 3.

the isotherm may reflect a kinetic effect on water adsorption (e.g., temperature dependence of sticking probability of water molecules).

The water coverage reaches to 1 ML at $\sim$15% RH and increases to 1.5 ML at 34% RH. Although the inflection point ($\sim$0.75 ML) close to 1 ML in the uptake curve of water might indicate a layer-by-layer growth of water on the hydroxylated $\alpha$-Fe$_2$O$_3$(0001) surface, inflection points at 2 and 3 ML at higher RHs than those in this study must be observed to confirm this argument. The uptake curve of water in this study is in quantitative agreement with the adsorption isotherm measured on hematite powders at 298 K using the volumetric method.[103]

*3.6.2. Spectral Features in O 1s XPS Spectra.* Next we discuss the changes in the binding energy and peak width of each component (H$_2$O/OH/Ox) in the O 1s XPS spectra of water-dosed $\alpha$-Fe$_2$O$_3$(0001). Two characteristic changes are observed in O 1s XPS spectra at higher RH's: (1) the peak position of OH shifts to lower BE, and (2) fwhm of the Ox peak decreases. Figure 6 shows (a) the chemical shift of OH relative to Ox, $\Delta E$(OH-Ox), and (b) fwhm of the Ox peak as a function of RH in the O 1s XPS spectra for the 1 Torr isobar on $\alpha$-Fe$_2$O$_3$(0001) shown in Figure 3. It should be noted that the chemical shift $\Delta E$(H$_2$O-Ox) and fwhm of adsorbed water remain constant in the RH range investigated in this study (RH $\leq$ 34%).

*3.6.2.1. Peak Shift of the OH Peak.* The chemical shift $\Delta E$(OH-Ox) in the 1 Torr isobar is about 1.55 eV at the low RH of $\sim$10$^{-3}$–10$^{-2}$ % and decreases to 1.35 eV at 0.12% RH, finally reaching a minimum of 1.05 eV at the high RH of $\sim$10% (see Figure 6a and Figure 3). The OH chemical shift of $\alpha$-Fe$_2$O$_3$(0001) at high RH's agrees well with previously reported OH chemical shifts of $\alpha$-FeOOH (1.1–1.3 eV).[78−81,95] There are a few possible explanations for the peak shift of OH observed at high RH's: (1) H-bonding of OH with water, (2) different types of OH species, and (3) surface reconstruction of the $\alpha$-Fe$_2$O$_3$(0001) surface.

Concerning explanation (1) above, it is noteworthy that $\sim$0.20 ML of adsorbed water is required on the surface to exhibit a distinguishable change ($>$0.10 eV) in the chemical shift of the OH peak. In the 1 Torr isobar (Figure 6a and

Figure 3), for example, the chemical shift $\Delta E$(OH-Ox) decreases from $\sim$1.55 to 1.35 eV at 0.12% RH where 0.16 ML H$_2$O is adsorbed on the surface. A similar relationship between the OH peak shift and water adsorption is found for other isobars at 0.1 and 0.02 Torr as well as for the isotherm at 295 K. Interestingly, upon H-bonding with adsorbed water, the O 1s XPS peak of OH groups on Cu(110) shifted to higher BE by 0.5 eV,[104] which is opposite to that observed for OH groups on $\alpha$-Fe$_2$O$_3$(0001) in the present study. In addition to Cu(110), the BE of OH groups on a Cu$_2$O thin film shifted to higher BE by 0.2 eV upon H-bonding with adsorbed water.[105] In contrast, no chemical shift was observed for OH species on TiO$_2$(110) upon H-bonding with water.[106] In general, OH species adsorbed on metal surfaces carry a partial negative charge that depends delicately on the interaction with the substrate.[107] This interaction makes OH on metal surfaces act as a Brønsted base in the H$_2$O(donor)−OH(acceptor) complex. The opposite peak shift of OH on $\alpha$-Fe$_2$O$_3$(0001) may be attributed to the different Brønsted acid/base character of OH groups and the different H-bonding nature of the H$_2$O−OH complex on $\alpha$-Fe$_2$O$_3$(0001) compared with metal surfaces such as Cu(110). To understand the complex behavior of OH species on $\alpha$-Fe$_2$O$_3$(0001) and other oxide surfaces like Cu$_2$O and TiO$_2$(110) upon water adsorption, however, it requires a theoretical study of the chemical bonding between OH and H$_2$O and the resulting change in electronic structure (i.e., chemical shift in XPS) using methods such as DFT.

Regarding explanation (2), which involved different types of OH species on the $\alpha$-Fe$_2$O$_3$(0001) surface, previous theoretical studies[40,58] showed that heterolytic dissociative adsorption (H$_2$O $\leftrightarrow$ OH$^-$ + H$^+$) is energetically favored over homolytic dissociative adsorption (H$_2$O $\leftrightarrow$ HO$^\bullet$ + 1/2 H$_2$). The heterolytic dissociation of water molecules on the $\alpha$-Fe$_2$O$_3$(0001) surface produces two types of surface hydroxyl groups. One OH species containing the oxygen atom of the water molecule is bonded to the iron atom on the $\alpha$-Fe$_2$O$_3$(0001) surface (HO-Fe); the other OH is formed by the attachment of the H fragment of the dissociated water molecule to a lattice oxygen (H−O$_{lattice}$) on the $\alpha$-Fe$_2$O$_3$(0001) surface. These different OH groups and/or these OH species with H-bonding to H$_2$O are in different chemical environments, which may also explain the observed peak shift of OH species on $\alpha$-Fe$_2$O$_3$(0001).

Concerning explanation (3), which involves surface reconstruction of $\alpha$-Fe$_2$O$_3$(0001) at high RH's, Trainor et al.[40] showed that the hydroxylated hematite surface at ambient conditions ($>$90% RH) consists of two distinct domains -a hydroxylated single-layer Fe termination and a hydroxylated oxygen termination. These differences in surface structure may be responsible for the observed peak shift of OH species in this study. Because there is no information available regarding the pressure (or RH) at which this surface reconstruction occurs, however, it is not clear whether surface reconstruction occurs at the lower RH conditions (RH $\leq$ 34%) in the present study.

*3.6.2.2. Peak Narrowing of the Oxide Peak.* Next we turn to the change in fwhm of the Ox peak as a function of RH. In the 1 Torr isobar (Figure 6b and Figure 3), the fwhm(Ox) decreases by $\sim$0.2 eV from 1.15 to 0.93 eV. The fwhm(Ox) decreases before the onset of water adsorption, which occurs at $\sim$3 $\times$ 10$^{-2}$ % RH in the 1 Torr isobar. The same trend is also observed for other isobars at 0.02 and 0.1 Torr. In the isotherm at 295 K (Figure 2), however, the fwhm(Ox) starts to decrease at substantially higher RH ($\sim$0.1% RH; $p$(H$_2$O) = 0.02 Torr at $T$ = 295 K) than the onset of water adsorption ($\sim$2 $\times$ 10$^{-5}$ %

RH; $\sim 5 \times 10^{-6}$ Torr at 295 K). Although the origin of the large difference in the onset of the fwhm(Ox) decrease between the isobars and the isotherm is not clear, the sharpening of the Ox peak at high RH's might be related to an adsorbate-induced surface core-level shift (SCLS). The core-level binding energy of surface atoms is shifted from that of bulk atoms due to the difference in the electronic distribution before core-hole excitation (initial-state effect) and the screening efficiency of core-holes (final-state effect).[108] In addition, the core-level binding energy of surface atoms is changed upon adsorption of surface chemical species on the clean surface. In the present case, the oxygen atoms on the clean $\alpha$-Fe$_2$O$_3$(0001) surface might produce a broadening of the Ox peak due to SCLS. On the adsorbate (OH and H$_2$O)-covered surface, the core-level binding energy of surface oxygen atoms may shift to that of OH or toward that of bulk oxygen atoms, which could lead to the decrease in fwhm(Ox).

As discussed above, it is not straightforward to clarify the origin of the OH peak shift and the narrowing of the Ox peak on $\alpha$-Fe$_2$O$_3$(0001) at high RH's. It would be beneficial to carry out DFT calculations on chemical shifts for OH groups at the different surface sites and on the reconstructed surface, and the change in chemical shifts of OH upon H-bonding to water. In addition, simulation of SCLS would be helpful in understanding the origin of the narrowing of the Ox peak. Indeed the recent study on the interaction of RuO$_2$(110) with molecular hydrogen using XPS and DFT calculations revealed in detail the different chemical shifts of OH groups at different surface sites as well as chemical shifts upon hydrogen bonding and the SCLS of surface oxygen species.[109]

***3.6.3. Comparison with the Previous ex Situ XPS Study.*** Here we compare results from the present in situ XPS study of hydroxylation and water adsorption on $\alpha$-Fe$_2$O$_3$(0001) at near ambient conditions with those from an earlier ex situ XPS study carried out by some of our coauthors.[30] The previous ex situ XPS study suggested that dissociative water adsorption on $\alpha$-Fe$_2$O$_3$(0001) occurs first at defect sites and then extensive hydroxylation proceeds at terrace sites above any threshold pressure of $\sim 10^{-4}$ Torr. As seen in Figures 2 and 4, the present study does not observe a distinct threshold pressure for hydroxylation on $\alpha$-Fe$_2$O$_3$(0001). It is noteworthy that there are a few distinct differences in the spectral features of O 1s XPS spectra between the present in situ XPS study and the previous ex situ XPS study. First, in the ex situ XPS study the chemical shift $\Delta E$(OH-Ox) is $\sim 1.5$ eV below the threshold water pressure, which is consistent with the $\Delta E$(OH-Ox) value observed in the present study at low RH's (1.5 eV) and in other earlier studies (1.4−1.6 eV).[28,32,63] Above the threshold water pressure, however, the OH peak was reported to shift to higher BE's and the $\Delta E$(OH-Ox) value increases to 1.9−2.2 eV. These observations are in contrast with results from the present study where the OH peak shifts to lower BEs and $\Delta E$(OH-Ox) decreases to 1.1 eV at high RHs. Second, the OH:Ox intensity ratio in the previous ex situ XPS study is $\sim 0.5$ below the threshold water pressure, which is again in agreement with the present study; however, the OH:Ox intensity ratio was found to increase dramatically up to 4.58 (2.89) above the threshold water pressure (for a 3 min, 9 (0.08) Torr exposure) in the previous ex situ study, which is much higher than the maximum OH:Ox ratio of 0.91 observed at the highest RH of 34% ($p$(H$_2$O) = 2 Torr at $T = 277$ K) in the present study. Using the multilayer model in this study, the coverage of OH on $\alpha$-Fe$_2$O$_3$(0001) is estimated to be 2.8 (2.2) ML from the OH:Ox ratio of 4.58 (2.89), which

indicates that hydroxylation must have proceeded into the subsurface region of $\alpha$-Fe$_2$O$_3$(0001) in the ex situ study.

This large difference in hydroxylation behavior between the in situ and ex situ XPS studies may have originated from the differences in the two samples: a cut and polished natural hematite crystal was used in the present study, whereas a thin film ($\sim 300$ Å) of hematite deposited on an $\alpha$-Al$_2$O$_3$(0001) substrate by oxygen-plasma-assisted molecular beam epitaxy was studied in the previous ex situ XPS study. In addition, the sample surface in the previous ex situ XPS study might have been covered by adventitious carbon after the sample was exposed to high water pressures in a transfer unit, although the coverage of C contamination was estimated to be less than 0.2 ML in the worst cases.[30] The large chemical shift of 1.9−2.2 eV observed in the previous ex situ XPS study can be well explained if oxygen-containing C contaminants such as methoxies, formates, and carboxylates were present on the thin-film hematite sample.[110,111] The origins of the large difference in hydroxylation behavior are not completely understood at this point.

## 4. Conclusions

Ambient pressure XPS was used to study the adsorption of water on the $\alpha$-Fe$_2$O$_3$(0001) surface under near ambient conditions up to 34% RH. We have found that water molecules are adsorbed on the hydroxylated $\alpha$-Fe$_2$O$_3$(0001) surface. Hydroxylation on $\alpha$-Fe$_2$O$_3$(0001) is initiated at the very low RH of $1 \times 10^{-7}$ % ($3 \times 10^{-8}$ Torr at 295 K). With an increase in RH, both OH and H$_2$O coverages increase. OH coverage increases up to 1 ML without any distinct threshold water pressure, as suggested in a previous ex situ XPS study.[30] A depth profiling experiment showed that hydroxylation occurs only at the topmost surface of $\alpha$-Fe$_2$O$_3$(0001) under our experimental conditions. Molecular water starts to adsorb on $\alpha$-Fe$_2$O$_3$(0001) at $\sim 2 \times 10^{-5}$ % RH at 295 K ($\sim 4 \times 10^{-6}$ Torr). The onset of water adsorption varies from $\sim 2 \times 10^{-5}$ to $\sim 4 \times 10^{-2}$ % RH depending on sample temperature and water pressure. H$_2$O coverage reaches 1 ML at $\sim 15$% RH and increases to 1.5 ML at the maximum RH of 34% in this study.

**Supporting Information Available:** Full description of the procedure for coverage calibration of carbon and other contaminants on $\alpha$-Fe$_2$O$_3$(0001). This material is available free of charge via the Internet at http://pubs.acs.org.

## References and Notes

(1) Brown, G. E., Jr.; Henrich, V. E.; Casey, W. H.; Clark, D. L.; Eggleston, C.; Felmy, A.; Goodman, D. W.; Gratzel, M.; Maciel, G.; McCarthy, M. I.; Nealson, K. H.; Sverjensky, D. A.; Toney, M. F.; Zachara, J. M. *Chem. Rev.* **1999**, *99*, 77.

(2) Cornell, R. M.; Schwertmann, U. *The Iron Oxides: Structure, Properties, Reactions, Occurrences, and Uses*, 2nd ed.; Wiley-VCH: Weinheim, Germany, 2003.

(3) Brown, G. E., Jr.; Trainor, T. P.; Chaka, A. M. In *Chemical Bonding at Surfaces and Interfaces*; Nilsson, A., Pettersson, L. G. M., Nørskov, J. K., Eds.; Elsevier: Amsterdam, 2008.

(4) Kocar, B. D.; Polizzotto, M. L.; Benner, S. G.; Ying, S. C.; Ung, M.; Ouch, K.; Samreth, S.; Suy, B.; Phan, K.; Sampson, M.; Fendorf, S. *Appl. Geochem.* **2008**, *23*, 3059.

(5) Tufano, K. J.; Reyes, C.; Saltikov, C. W.; Fendorf, S. *Environ. Sci. Technol.* **2008**, *42*, 8283.

(6) Geus, J. W. *Appl. Catal.* **1986**, *25*, 313.

(7) Muhler, M.; Schlögl, R.; Ertl, G. *J. Catal.* **1992**, *138*, 413.

(8) Hradil, D.; Grygar, T. V.; Hradilová, J.; Bezdička, P. *Appl. Clay Sci.* **2003**, *22*, 223.

(9) Suri, K.; Annapoorni, S.; Sarkar, A. K.; Tandon, R. P. *Sens. Actuator B* **2002**, *81*, 277.

(10) Khader, M. M.; Vurens, G. H.; Kim, I.-K.; Salmeron, M.; Somorjai, G. A. *J. Am. Chem. Soc.* **1987**, *109*, 3581.

(11) Kay, A.; Cesar, I.; Grätzel, M. *J. Am. Chem. Soc.* **2006**, *128*, 15714.

(12) Mallinson, J. C. *The Foundations of Magnetic Recording*; Academic Press: Boston, 1993.

(13) Thiel, P. A.; Madey, T. E. *Surf. Sci. Rep.* **1987**, *7*, 211.

(14) Henderson, M. A. *Surf. Sci. Rep.* **2002**, *46*, 1.

(15) Chorkendorff, I.; Niemantsverdriet, J. W. *Concepts of Modern Catalysis and Kinetics*; Wiley-VCH: Weinheim, 2003.

(16) Navrotsky, A.; Mazeina, L.; Majzlan, J. *Science* **2008**, *319*, 1635.

(17) Pauling, L.; Hendricks, S. B. *J. Am. Chem. Soc.* **1925**, *47*, 781.

(18) Kurtz, R. L.; Henrich, V. E. *Surf. Sci.* **1983**, *129*, 345.

(19) Hendewerk, M.; Salmeron, M.; Somorjai, G. A. *Surf. Sci.* **1986**, *172*, 544.

(20) Kurtz, R. L.; Henrich, V. E. *Phys. Rev. B* **1987**, *36*, 3413.

(21) Lad, R. J.; Henrich, V. E. *Surf. Sci.* **1988**, *193*, 81.

(22) Eggleston, C. M.; Hochella, M. F., Jr. *Am. Mineral.* **1992**, *77*, 911.

(23) Barbieri, A.; Weiss, W.; Van Hove, M. A.; Somorjai, G. A. *Surf. Sci.* **1994**, *302*, 259.

(24) Condon, N. G.; Murray, P. W.; Leibsle, F. M.; Thornton, G.; Lennie, A. R.; Vaughan, D. J. *Surf. Sci.* **1994**, *310*, L609.

(25) Condon, N. G.; Leibsle, F. M.; Lennie, A. R.; Murray, P. W.; Vaughan, D. J.; Thornton, G. *Phys. Rev. Lett.* **1995**, *75*, 1961.

(26) Guo, Q. L.; Gui, L. L.; Wu, N. Z. *Appl. Surf. Sci.* **1996**, *99*, 229.

(27) Møller, P. J.; Guo, Q. L.; Gui, L. L. *Thin Solid Films* **1996**, *281−282*, 76.

(28) Junta-Rosso, J. L.; Hochella, M. F., Jr. *Geochim. Cosmochim. Acta* **1996**, *60*, 305.

(29) Condon, N. G.; Leibsle, F. M.; Lennie, A. R.; Murray, P. W.; Parker, T. M.; Vaughan, D. J.; Thornton, G. *Surf. Sci.* **1998**, *397*, 278.

(30) Liu, P.; Kendelewicz, T.; Brown, G. E., Jr.; Nelson, E. J.; Chambers, S. A. *Surf. Sci.* **1998**, *417*, 53.

(31) Chambers, S. A.; Yi, S. I. *Surf. Sci.* **1999**, *439*, L785.

(32) Thevuthasan, S.; Kim, Y. J.; Yi, S. I.; Chambers, S. A.; Morais, J.; Denecke, R.; Fadley, C. S.; Liu, P.; Kendelewicz, T.; Brown, G. E., Jr. *Surf. Sci.* **1999**, *425*, 276.

(33) Shaikhutdinov, S. K.; Weiss, W. *Surf. Sci.* **1999**, *432*, L627.

(34) Ketteler, G.; Weiss, W.; Ranke, W.; Schlögl, R. *Phys. Chem. Chem. Phys.* **2001**, *3*, 1114.

(35) Ketteler, G.; Weiss, W.; Ranke, W. *Surf. Rev. Lett.* **2001**, *8*, 661.

(36) Weiss, W.; Ranke, W. *Prog. Surf. Sci.* **2002**, *70*, 1.

(37) Leist, U.; Ranke, W.; Al-Shamery, K. *Phys. Chem. Chem. Phys.* **2003**, *5*, 2435.

(38) Eggleston, C. M.; Stack, A. G.; Rosso, K. M.; Higgins, S. R.; Bice, A. M.; Boese, S. W.; Pribyl, R. D.; Nichols, J. J. *Geochim. Cosmochim. Acta* **2003**, *67*, 985.

(39) Kim, C.-Y.; Escuadro, A. A.; Bedzyk, M. J.; Liu, L.; Stair, P. C. *Surf. Sci.* **2004**, *572*, 239.

(40) Trainor, T. P.; Chaka, A. M.; Eng, P. J.; Newville, M.; Waychunas, G. A.; Catalano, J. G.; Brown, G. E., Jr. *Surf. Sci.* **2004**, *573*, 204.

(41) Lemire, C.; Bertarione, S.; Zecchina, A.; Scarano, D.; Chaka, A.; Shaikhutdinov, S.; Freund, H.-J. *Phys. Rev. Lett.* **2005**, *94*, 166101.

(42) Barbier, A.; Stierle, A.; Kasper, N.; Guittet, M.-J.; Jupille, J. *Phys. Rev. B* **2007**, *75*, 233406.

(43) Lübbe, M.; Moritz, W. *J. Phys.: Condens. Matter* **2009**, *21*, 134010.

(44) Becker, U.; Hochella, M. F., Jr.; Aprà, E. *Am. Mineral.* **1996**, *81*, 1301.

(45) Wasserman, E.; Rustad, J. R.; Felmy, A. R.; Hay, B. P.; Halley, J. W. *Surf. Sci.* **1997**, *385*, 217.

(46) Wang, X. G.; Weiss, W.; Shaikhutdinov, S. K.; Ritter, M.; Petersen, M.; Wagner, F.; Schlögl, R.; Scheffler, M. *Phys. Rev. Lett.* **1998**, *81*, 1038.

(47) Parker, S. C.; de Leeuw, N. H.; Redfern, S. E. *Faraday Discuss.* **1999**, *114*, 381.

(48) Jones, F.; Rohl, A. L.; Farrow, J. B.; van Bronswijk, W. *Phys. Chem. Chem. Phys.* **2000**, *2*, 3209.

(49) Lado-Touriño, I.; Tsobnang, F. *Comput. Mater. Sci.* **2000**, *17*, 243.

(50) Warschkow, O.; Ellis, D. E.; Hwang, J. H.; Mansourian-Hadavi, N.; Mason, T. O. *J. Am. Ceram. Soc.* **2002**, *85*, 213.

(51) Rohrbach, A.; Hafner, J.; Kresse, G. *Phys. Rev. B* **2004**, *70*, 125426.

(52) Rollmann, G.; Rohrbach, A.; Entel, P.; Hafner, J. *Phys. Rev. B* **2004**, *69*, 165107.

(53) Alvarez-Ramírez, F.; Martínez-Magadán, J. M.; Gomes, J. R. B.; Illas, F. *Surf. Sci.* **2004**, *558*, 4.

(54) Bergermayer, W.; Schweiger, H.; Wimmer, E. *Phys. Rev. B* **2004**, *69*, 195409.

(55) Spagnoli, D.; Cooke, D. J.; Kerisit, S.; Parker, S. C. *J. Mater. Chem.* **2006**, *16*, 1997.

(56) de Leeuw, N. H.; Cooper, T. G. *Geochim. Cosmochim. Acta* **2007**, *71*, 1655.

(57) Jarvis, E. A.; Chaka, A. M. *Surf. Sci.* **2007**, *601*, 1909.

(58) Yin, S. X.; Ma, X. Y.; Ellis, D. E. *Surf. Sci.* **2007**, *601*, 2426.

(59) Yin, S. X.; Ellis, D. E. *Surf. Sci.* **2008**, *602*, 2047.

(60) Goniakowski, J.; Finocchi, F.; Noguera, C. *Rep. Prog. Phys.* **2008**, *71*, 016501.

(61) Barbier, A.; Stierle, A.; Finocchi, F.; Jupille, J. *J. Phys.: Condens. Matter* **2008**, *20*, 184014.

(62) Brundle, C. R.; Chuang, T. J.; Wandelt, K. *Surf. Sci.* **1977**, *68*, 459.

(63) Mills, P.; Sullivan, J. L. *J. Phys. D: Appl. Phys.* **1983**, *16*, 723.

(64) Fujii, T.; de Groot, F. M. F.; Sawatzky, G. A.; Voogt, F. C.; Hibma, T.; Okada, K. *Phys. Rev. B* **1999**, *59*, 3195.

(65) Kuiper, P.; Searle, B. G.; Rudolf, P.; Tjeng, L. H.; Chen, C. T. *Phys. Rev. Lett.* **1993**, *70*, 1549.

(66) Crocombette, J. P.; Pollak, M.; Jollet, F.; Thromat, N.; Gautier-Soyer, M. *Phys. Rev. B* **1995**, *52*, 3143.

(67) Ogletree, D. F.; Bluhm, H.; Lebedev, G.; Fadley, C. S.; Hussain, Z.; Salmeron, M. *Rev. Sci. Instrum.* **2002**, *73*, 3872.

(68) Bluhm, H.; Andersson, K.; Araki, T.; Benzerara, K.; Brown, G. E.; Dynes, J. J.; Ghosal, S.; Gilles, M. K.; Hansen, H. C.; Hemminger, J. C.; Hitchcock, A. P.; Ketteler, G.; Kilcoyne, A. L. D.; Kneedler, E.; Lawrence, J. R.; Leppard, G. G.; Majzlam, J.; Mun, B. S.; Myneni, S. C. B.; Nilsson, A.; Ogasawara, H.; Ogletree, D. F.; Pecher, K.; Salmeron, M.; Shuh, D. K.; Tonner, B.; Tyliszczak, T.; Warwick, T.; Yoon, T. H. *J. Electron Spectrosc. Relat. Phenom.* **2006**, *150*, 86.

(69) Bluhm, H.; Hävecker, M.; Knop-Gericke, A.; Kiskinova, M.; Schlögl, R.; Salmeron, M. *MRS Bull.* **2007**, *32*, 1022.

(70) Salmeron, M.; Schlögl, R. *Surf. Sci. Rep.* **2008**, *63*, 169.

(71) Yamamoto, S.; Bluhm, H.; Andersson, K.; Ketteler, G.; Ogasawara, H.; Salmeron, M.; Nilsson, A. *J. Phys.: Condens. Matter* **2008**, *20*, 184025.

(72) Ogletree, D. F.; Bluhm, H.; Hebenstreit, E. D.; Salmeron, M. *Nucl. Instrum. Methods Phys. Res. A* **2009**, *601*, 151.

(73) *CRC Handbook of Chemistry and Physics*, 61st ed.; CRC Press: Boca Raton, FL, 1981.

(74) Shirley, D. A. *Phys. Rev. B* **1972**, *5*, 4709.

(75) McCafferty, E.; Wightman, J. P. *Surf. Interface Anal.* **1998**, *26*, 549.

(76) Andersson, K.; Nikitin, A.; Pettersson, L. G. M.; Nilsson, A.; Ogasawara, H. *Phys. Rev. Lett.* **2004**, *93*, 196101.

(77) Faradzhev, N. S.; Kostov, K. L.; Feulner, P.; Madey, T. E.; Menzel, D. *Chem. Phys. Lett.* **2005**, *415*, 165.

(78) McIntyre, N. S.; Zetaruk, D. G. *Anal. Chem.* **1977**, *49*, 1521.

(79) Wandelt, K. *Surf. Sci. Rep.* **1982**, *2*, 1.

(80) Junta, J. L.; Hochella, M. F., Jr. *Geochim. Cosmochim. Acta* **1994**, *58*, 4985.

(81) Temesghen, W.; Sherwood, P. M. A. *Anal. Bioanal. Chem.* **2002**, *373*, 601.

(82) Chambers, S. A.; Joyce, S. A. *Surf. Sci.* **1999**, *420*, 111.

(83) Herman, G. S.; McDaniel, E. P.; Joyce, S. A. *J. Electron Spectrosc. Relat. Phenom.* **1999**, *101−103*, 433.

(84) Cutting, R. S.; Muryn, C. A.; Vaughan, D. J.; Thornton, G. *Surf. Sci.* **2008**, *602*, 1155.

(85) Joseph, Y.; Ranke, W.; Weiss, W. *J. Phys. Chem. B* **2000**, *104*, 3224.

(86) Himpsel, F. J.; McFeely, F. R.; Taleb-Ibrahimi, A.; Yarmoff, J. A.; Hollinger, G. *Phys. Rev. B* **1988**, *38*, 6084.

(87) Kurbatov, G.; Darque-Ceretti, E.; Aucouturier, M. *Surf. Interface Anal.* **1992**, *18*, 811.

(88) Powell, C. J.; Jablonski, A. *NIST Electron Inelastic-Mean-Free-Path Database*, version 1.1; National Institute of Standards and Technology: Gaithersburg, MD, 2000.

(89) Tanuma, S.; Powell, C. J.; Penn, D. R. *Surf. Interface Anal.* **1988**, *11*, 577.

(90) Coe, J. V.; Earhart, A. D.; Cohen, M. H.; Hoffman, G. J.; Sarkas, H. W.; Bowen, K. H. *J. Chem. Phys.* **1997**, *107*, 6023.

(91) Leland, J. K.; Bard, A. J. *J. Phys. Chem.* **1987**, *91*, 5076.

(92) Mogili, P. K.; Kleiber, P. D.; Young, M. A.; Grassian, V. H. *J. Phys. Chem. A* **2006**, *110*, 13799.

(93) Rahaman, A.; Grassian, V. H.; Margulis, C. J. *J. Phys. Chem. C* **2008**, *112*, 2109.

(94) Thomas, A. C.; Richardson, H. H. *J. Phys. Chem. C* **2008**, *112*, 20033.

(95) Welsh, I. D.; Sherwood, P. M. A. *Phys. Rev. B* **1989**, *40*, 6386.

(96) Shannon, R. D. *Acta Crystallogr., Sect. A* **1976**, *32*, 751.

(97) Andersson, K.; Ketteler, G.; Bluhm, H.; Yamamoto, S.; Ogasawara, H.; Pettersson, L. G. M.; Salmeron, M.; Nilsson, A. *J. Am. Chem. Soc.* **2008**, *130*, 2793.

(98) Giordano, L.; Goniakowski, J.; Suzanne, J. *Phys. Rev. Lett.* **1998**, *81*, 1271.

(99) Hass, K. C.; Schneider, W. F.; Curioni, A.; Andreoni, W. *Science* **1998**, *282*, 265.

(100) Odelius, M. *Phys. Rev. Lett.* **1999**, *82*, 3919.

(101) Morimoto, T.; Nagao, M.; Tokuda, F. *J. Phys. Chem.* **1969**, *73*, 243.

(102) McCafferty, E.; Zettlemoyer, A. C. *Discuss. Faraday Soc.* **1971**, *52*, 239.

(103) McCafferty, E.; Zettlemoyer, A. C. *J. Colloid Interface Sci.* **1970**, *34*, 452.

(104) Andersson, K.; Ketteler, G.; Bluhm, H.; Yamamoto, S.; Ogasawara, H.; Pettersson, L. G. M.; Salmeron, M.; Nilsson, A. *J. Phys. Chem. C* **2007**, *111*, 14493.

(105) Deng, X.; Herranz, T.; Weis, C.; Bluhm, H.; Salmeron, M. *J. Phys. Chem. C* **2008**, *112*, 9668.

(106) Ketteler, G.; Yamamoto, S.; Bluhm, H.; Andersson, K.; Starr, D. E.; Ogletree, D. F.; Ogasawara, H.; Nilsson, A.; Salmeron, M. *J. Phys. Chem. C* **2007**, *111*, 8278.

(107) Schiros, T.; Näslund, L.-Å.; Andersson, K.; Gyllenpalm, J.; Karlberg, G. S.; Odelius, M.; Ogasawara, H.; Pettersson, L. G. M.; Nilsson, A. *J. Phys. Chem. C* **2007**, *111*, 15003.

(108) Mårtensson, N.; Nilsson, A. In *Application of Synchrotron Radiation*; Eberhardt, W., Ed.; Springer: Berlin, 1995; Vol. 35, p 65.

(109) Knapp, M.; Crihan, D.; Seitsonen, A. P.; Lundgren, E.; Resta, A.; Andersen, J. N.; Over, H. *J. Phys. Chem. C* **2007**, *111*, 5363.

(110) Onishi, H.; Egawa, C.; Aruga, T.; Iwasawa, Y. *Surf. Sci.* **1987**, *191*, 479.

(111) Mullins, D. R.; Robbins, M. D.; Zhou, J. *Surf. Sci.* **2006**, *600*, 1547.